Highly conductive paper for energy-storage devices

Liangbing Hu[a,1], Jang Wook Choi[a,1], Yuan Yang[a,1], Sangmoo Jeong[b], Fabio La Mantia[a], Li-Feng Cui[a], and Yi Cui[a,2]

Departments of [a]Materials Science and Engineering and [b]Electrical Engineering, Stanford University, Stanford, CA 94305

Edited by Charles M. Lieber, Harvard University, Cambridge, MA, and approved October 21, 2009 (received for review August 6, 2009)

Paper, invented more than 2,000 years ago and widely used today in our everyday lives, is explored in this study as a platform for energy-storage devices by integration with 1D nanomaterials. Here, we show that commercially available paper can be made highly conductive with a sheet resistance as low as 1 ohm per square (Ω/sq) by using simple solution processes to achieve conformal coating of single-walled carbon nanotube (CNT) and silver nanowire films. Compared with plastics, paper substrates can dramatically improve film adhesion, greatly simplify the coating process, and significantly lower the cost. Supercapacitors based on CNT-conductive paper show excellent performance. When only CNT mass is considered, a specific capacitance of 200 F/g, a specific energy of 30–47 Watt-hour/kilogram (Wh/kg), a specific power of 200,000 W/kg, and a stable cycling life over 40,000 cycles are achieved. These values are much better than those of devices on other flat substrates, such as plastics. Even in a case in which the weight of all of the dead components is considered, a specific energy of 7.5 Wh/kg is achieved. In addition, this conductive paper can be used as an excellent lightweight current collector in lithium-ion batteries to replace the existing metallic counterparts. This work suggests that our conductive paper can be a highly scalable and low-cost solution for high-performance energy storage devices.

conformal coating | carbon nanotubes | nanomaterial | solution process

Printable solution processing has been exploited to deposit various nanomaterials, such as fullerene, carbon nanotubes (CNTs), nanocrystals, and nanowires for large-scale applications, including thin-film transistors (1–3), solar cells (4, 5), and energy-storage devices (6, 7), because the process is low-cost while maintaining the unique properties of the nanomaterials. In these processes, flat substrates, such as glass, metallic films, Si wafers, and plastics, have been used to hold nanostructure films. Nanostructured materials are usually first capped with surfactant molecules so that they can be well-dispersed as separated particles in a solvent to form "ink." The ink is then deposited onto the flat substrates, followed by surfactant removal and solvent evaporation. To produce high-quality films, significant efforts have been spent on ink formulation and rheology adjustment. Moreover, because the surfactants are normally insulating, and thus limit the charge transfer between the nanomaterials, their removal is particularly critical. However, this step involves extensive washing and chemical displacement, which often cause mechanical detachment of the film from the flat substrate. Polymer binders or adhesives have been used to improve the binding of nanomaterials to substrates, but these can also cause an undesirable decrease in the film conductivity. These additional procedures increase the complexity of solution processing and result in high cost and low throughput. Here, we exploit paper substrates used in daily life to solve these issues and develop a simple, low-cost, high-throughput, and printable process for achieving superior device performance.

Throughout human history, paper has been the most important medium to express and propagate information and knowledge. The Prisse Papyrus, the oldest existing piece of writing on paper, dates back to 2,000 B.C. (8). The critical feature that enables paper to record information in such an enduring manner is the strong adhesion of ink onto paper, resulting from the 3D hierarchical porous fiber structures, surface charges, and functional groups in paper, which are under fine control today (9). Paper has continued to expand its applications beyond information recording, and recently, novel applications such as microfluidic and electronic devices have been demonstrated. Whitesides and colleagues fabricated 3D microfluidic devices by stacking paper and adhesive tape (10) and, in a separate study, portable bioassays on patterned paper substrates (11). Researchers in the flexible electronics community have also explored paper as substrates for organic photodiodes (12), organic thin-film transistors (13, 14), circuits (15), and active matrix displays (16). In this study, we demonstrated that the application of paper can be expanded even further to important energy-storage devices by integrating with single-walled CNTs and metal nanowires by solution-based processes. The coated 1D nanomaterial films show high conductivity, high porosity, and robust chemical and mechanical stability, which lead to high-performance supercapacitors (SCs) and lithium-ion (Li-ion) batteries.

Results and Discussion

Aqueous CNT ink with sodium dodecylbenzenesulfonate (SDBS) as a surfactant was used in this study (17), where SDBS and CNT were 10 and 1–5 mg/mL in concentration, respectively. Once CNT ink was applied onto paper by the simple Meyer rod coating method (Fig. 1*A*), the paper was transformed into highly conductive paper with a low sheet resistance around 10 Ω/sq (Fig. 1*B*), which is lower than previous reports by several orders of magnitude because of the ink formulation and the choice of substrates (18, 19). Fig. 1 *C* and *D* shows the conformal coating of CNTs on the fiber structure of the paper, which contributes to high film conductivity (see Figs. S1 and S2 for more details). One important reason for this conformal coating might be the porous structure of paper, which leads to large capillary force for the ink. The strong capillary force enables high contacting surface area between flexible nanotubes and paper after the solvent is absorbed and dried out. We also applied the same method to produce conductive paper based on ink of other nanoscale materials, by using Ag NWs as an example (Fig. 1*E* and Table S1; see *Materials and Methods* for detailed procedures). The sheet resistances at different effective film thicknesses for CNTs and Ag NWs are plotted in Fig. 1*F*. Benefitting from the conformal coating, the sheet resistances reached a low level of 1 Ω/sq for Ag NWs at the effective film thickness of 500 nm. As film thickness increased, the scaling of the resistance changed from percolation-like to linear behavior, which is similar to CNT networks on flat substrates. The cross-over from percolation to linear region was found to be ≈20–30 nm on other flat substrates, which is close to our value, ≈10 nm (Fig. 1*F*), and the difference is likely due to the length differences of CNTs (20, 21).

Author contributions: L.H., J.W.C., Y.Y., and Y.C. designed research; L.H., J.W.C., Y.Y., S.J., F.L.M., and L.-F.C. performed research; L.H., J.W.C., Y.Y., and Y.C. analyzed data; and L.H., J.W.C., Y.Y., and Y.C. wrote the paper.

The authors declare no conflict of interest.

This article is a PNAS Direct Submission.

[1]L.H., J.W.C., and Y.Y. contributed equally to this work.

[2]To whom correspondence should be addressed. E-mail: yicui@stanford.edu.

This article contains supporting information online at www.pnas.org/cgi/content/full/0908858106/DCSupplemental.

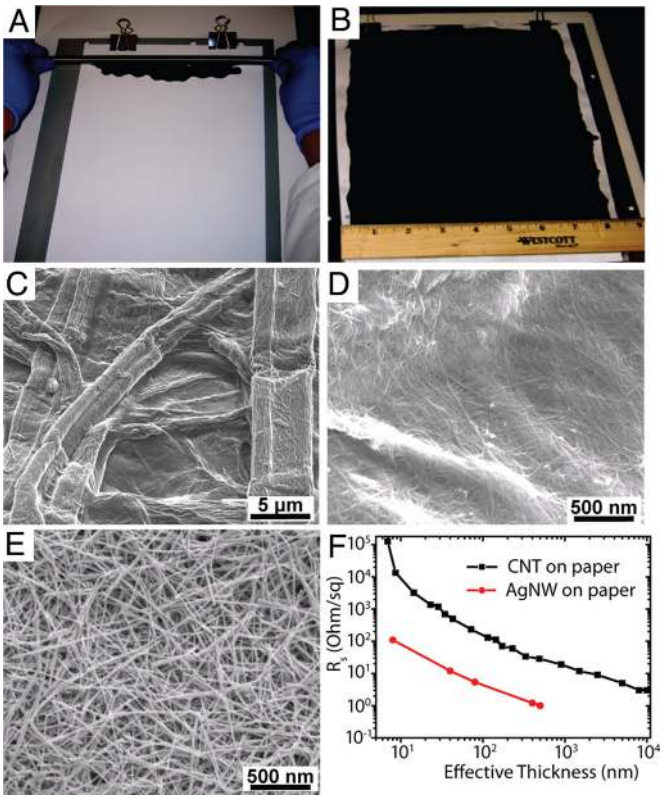

Fig. 1. Conformal coating of CNTs or Ag NWs on commercial paper. (*A*) Meyer rod coating of CNT or Ag NW ink on commercial Xerox paper. (*B*) Conductive Xerox paper after CNT coating with sheet resistance of ≈10 Ω/sq. SEM images of (*C*) surface morphology of Xerox paper, (*D*) conformal CNT coating along fibers in Xerox paper, and (*E*) conformal Ag NW coating on Xerox paper. (*F*) Sheet resistances of conductive paper based on CNTs and Ag NWs with various thicknesses.

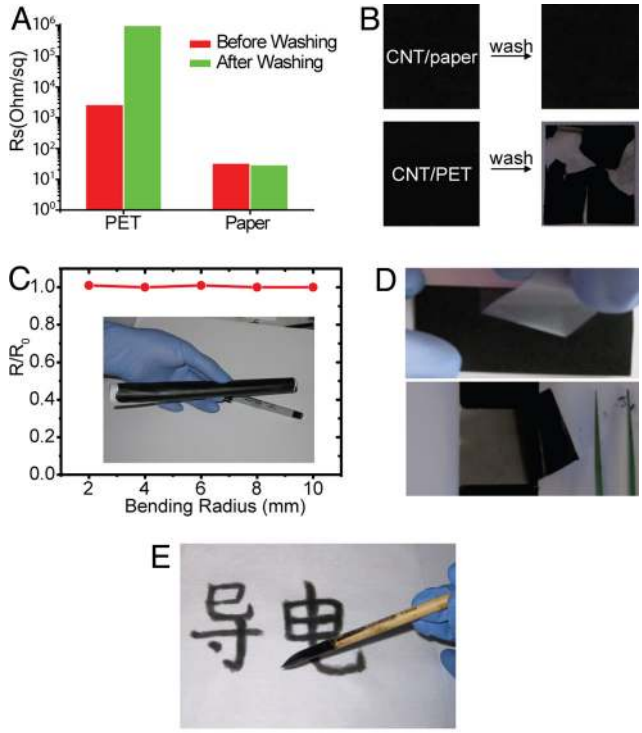

Fig. 2. Various performance tests of conductive paper. (*A*) Sheet resistance change of CNTs on paper and PET before and after the process of washing to remove surfactants. (*B*) The comparison of film peeling after washing surfactants. CNT films on PET are easily peeled off, whereas CNTs on paper still stick well. (*C*) Sheet resistance changes after bending conductive paper into different radii. (*D*) Film adhesion test with Scotch tape: CNTs on paper remain bound, whereas CNTs on PET are peeled off. (*E*) Direct writing of CNT ink on the paper with Chinese calligraphy.

Because paper absorbs solvents easily and binds with CNTs strongly, the fabrication process for the conductive paper is much simpler than that for other flat substrates, such as glass or plastics. First, contrary to other substrates, ink rheology for paper is not strict at all. In glass and plastics, the ink surface energy needs to match with that of substrates, and the viscosity must be high enough to avoid surface tension-driven defects, such as rings and dewetting in the coating and drying processes (22). Therefore, various additives are incorporated in the ink to tune the rheology properties. These insulating additives decrease the conductivity of the final film. In contrast, our CNT ink does not need any additives to adjust the rheology, which simplifies the process and leads to high film conductivity. Second, the paper does not require surfactant washing processes to achieve high film conductivity, which is necessary for other substrates. As shown in Fig. 2 *A* and *B*, the sheet resistance of the CNT paper was already as low as 30 Ω/sq before washing, and there was no film delamination and sheet resistance change after washing. In contrast, washing of CNTs on Polyethylene terephthalate (PET) substrates resulted in significant film cracking and peel-off (Fig. 2*B*). The local resistance of CNT film on PET decreased significantly (Fig. S3*A*); however, the global resistance became ≈1,000 times higher (Fig. 2*A*). Although the detailed mechanism behind this unusual phenomenon is unclear, it is likely that while solvent is sucked into paper by capillary force, surfactants become rearranged, perhaps toward porous fiber networks, such that surfactants do not hinder charge transport within CNT films as much as they do with flat substrates. This unusual property of paper renders the typical surfactant washing requirement unnecessary in the case of conductive paper, and thus its fabrication process becomes greatly simplified.

The conductive paper also has excellent mechanical properties. The conductive paper with CNT thicknesses from 100 nm to 5 μm can be bent down to a 2-mm radius (Fig. 2*C*) or folded without any measurable change in electrical conductivity. Fatigue tests show that the conductive paper can be bent to a 2-mm radius for 100 times with resistance increase less than 5%. These mechanical behaviors are likely due to the combined effect of the flexibility of individual CNTs, the strong binding of the CNTs with the paper fibers, and the porous morphology of the paper, which can relax the bending strain. Such flexibility could satisfy the requirement in SCs and batteries. In comparison, conductive paper with a 50-nm gold layer evaporated on Xerox paper showed R_s of 7 Ω/sq. The sheet resistance increased by 50% after folding the conductive gold paper three times. Moreover, the strong adhesion of the CNTs to paper lead to high film stability against damage, such as scratching and peeling-off. This is demonstrated via a Scotch tape test showing the clear superiority of using paper over the PET substrate (Fig. 2*D*). The Scotch tape did not peel off any CNTs on paper, and the sheet resistance remained the same, ≈10 Ω/sq. As in the conformal coating, the exceptionally strong binding is attributed to the large capillary force and maximized contact area and, subsequently, Van der Waals force between the CNTs and paper (23). The superior flexibility and high stability make conductive paper promising for various rolled-up devices. It is noteworthy that the conductive paper described here is completely distinct from previously reported bulky papers (24) or other conductive paper (25) in several perspectives. (*i*) We used widely available commercial paper, not paper-like films produced by more complicated processes. Therefore, we could

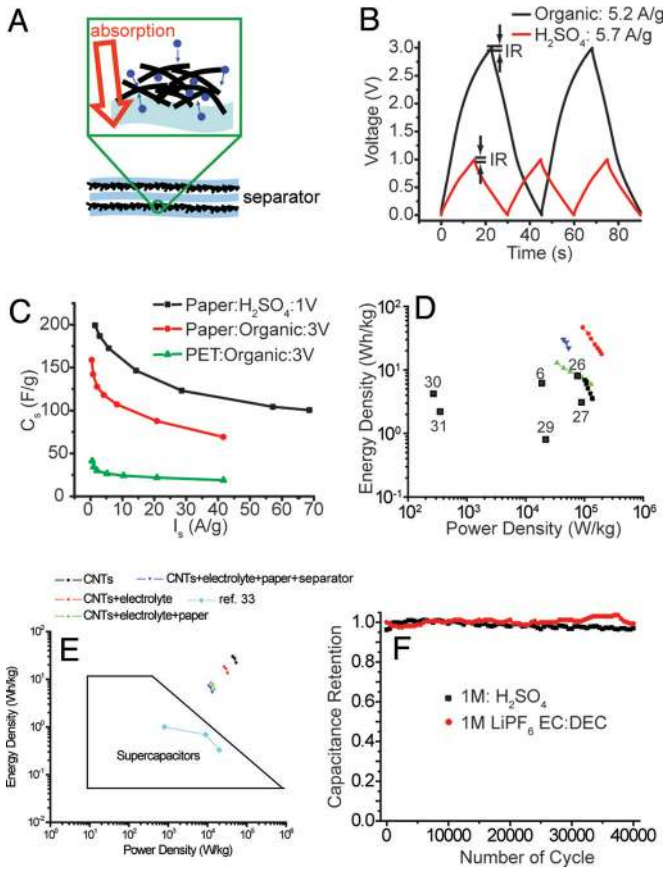

Fig. 3. Conductive paper as SC electrodes. (*A*) Schematic illustration of all-paper SCs based on CNT conductive paper. Zoomed-in schematic illustrates that ion accessibility is enhanced by the strong solvent absorption. (*B*) Galvanostatic charging/discharging curves taken from 3 V with organic electrolyte and 1 V with sulfuric acid. (*C*) Gravimetric capacitances at various currents measured in aqueous and organic electrolytes. Data from CNTs on PET are plotted together for comparison. (*D*) A Ragone plot showing that the all-paper SCs outperform the PET SC devices and reported data in literature (6, 26, 27, 30, 31). The color coding (black, red, green) of the traces is the same as in *C*. Data in *B*–*D* as well as data from references mentioned in *D* are calculated based on a mass loading of CNTs only. Typical mass CNT loadings in *C* and *D* are 72 μg/cm^2, and data from a large mass loading of 1.7 mg/cm^2 are also presented (*D*, blue plot). (*E*) A Ragone plot based on the mass of different combinations of dead components. A plot from ref. 33 based on the mass of entire device components is also presented. The trapezoid showing the performance of commercial devices is from ref. 36. (*F*) Capacitance retention measured in different electrolytes. After 40,000 cycles, 97% and 99.4% of initial capacitances are maintained for sulfuric acid and organic electrolytes, respectively.

benefit from the well-established paper technology. (*ii*) Our conductive paper takes advances of intrinsic properties of paper, which largely simplifies the fabrication process. (*iii*) Our fabrication process is scalable, with roll-to-roll fashion. (*iv*) Other painting methods can also be applied to fabricate conductive paper. Chinese calligraphy (Fig. 2*E*) and pen writing (Fig. S3*B*) are demonstrated as examples.

Because of the high conductivity and the large surface area, the conductive paper was studied in SC applications as active electrodes and current collectors. CNTs deposited on porous paper are more accessible to ions in the electrolyte than those on flat substrates (6, 26–33), which can result in high power density. In addition, the paper itself can function well as a separator. Therefore, all-paper SCs have been realized by simple fabrication processes (Fig. 3*A*). We fabricated such all-paper SCs and tested their performance in both aqueous and organic electrolytes by using galvanostatic (Fig. 3*B*) and cyclic voltammetric (Fig. S5) methods. Detailed procedures for the device preparation and performance characterization are described in *Materials and Methods* and *SI Materials and Methods*. As shown in Fig. 3*C*, the specific capacitances of all-paper SCs at various currents are superior to the previously reported values with pure CNT electrodes on flat substrates (6, 26–33), and are even close to those of pseudocapacitors based on the polymer/CNT composites (34, 35). A high specific capacitance of 200 F/g was achieved for devices in sulfuric acid electrolyte (Fig. 3*C*). Furthermore, our devices can maintain excellent specific capacitance even under high-current operations. Even at ≈40 A/g, capacitances larger than 70 F/g were maintained in both aqueous and organic phases. Such high capacitances at large currents are attributed to the excellent ion accessibility from both sides of the CNT film and intimate electrolyte–CNT wetting that originates from the porous nature of paper. For comparison, PET-based SCs prepared in the same way only showed capacity less than 50 F/g, (Fig. 3*C*), which indicates the importance of the porous nature of paper for better SC performance. This is also confirmed by another control experiment with Au conductive paper. Devices with the same amount of CNTs on Au-coated Xerox paper (50 nm, 7 Ω/sq) showed 36 F/g at 10 A/g, which is 4 ≈ 5-fold lower than our CNT conductive paper SCs (≈160 F/g at the same current density). This is likely because the Au film blocks pores in paper and impedes the ion access from the paper side. When operated at 3 V in organic solvent, the specific energy and power reached 47 Wh/kg and 200,000 W/kg, respectively, which exceed previously reported data (Fig. 3*D*) (6, 26, 27, 30, 31). Our data in this plot are calculated based on CNT mass only to compare with other data in the references that were also acquired in the same way. Furthermore, even in a case when CNT mass loading increased to 1.7 mg/cm^2, the device performance was still superior to others reported (Fig. 3*D*). The superior capacitances may be a result of the higher ion accessibility in the paper due to the strong absorption of solvent by the paper. The CNT film on paper is also thinner, with the same mass loading as a result of the larger surface area of the rough paper. Also, to compare with commercial devices (36) and see the significance of mass saving by replacing metal current collectors with conductive paper, we plotted another Ragone plot (Fig. 3*E*). In this plot, the mass of dead components (electrolyte, paper, separator = 1.1, 3.3, 1.6 mg/cm^2, respectively) was considered in addition to active materials (CNTs = 1.7 mg/cm^2). This Ragone plot shows that our data are better in both energy/power densities compared with commercial devices as well as reported data in the literature (33) that are also based on the mass of all of the device components.

Cycle life, one of the most critical parameters in the SC operations, turns out to be excellent for 40,000 cycles (Fig. 3*F*). Only 3% and 0.6% capacitance losses were observed in sulfuric acid and organic electrolyte, respectively. Moreover, the conductive paper was mechanically robust and did not show any cracks or evidence of breakage for 60 days. CNT films as thick as ≈14 μm (1.33 mg/cm^2) were also tested in sulfuric acid, and capacitances as high as ≈122 F/g were achieved (Fig. S6*B*). The devices with 1.33 and 1.7 mg/cm^2 CNTs were compared with the reported densest CNT assembly data (Fig. S6*C*) (28). Our devices show larger capacitances per area compared with their films, although their films are 10 times thicker. Furthermore, their devices also leave plenty of unused space, and therefore might not be scalable. More data on cyclic voltammetry (CV; Fig. S5) and thickness dependence of the capacitance (Fig. S6*A*) are presented in the *SI Materials and Methods*.

Rechargeable batteries are another type of energy-storage device with high energy density, but they are still too heavy for applications such as vehicle electrification. In this work, conductive paper was used to replace the heavy metallic current collectors, which could reduce the weight of batteries up to 20% (Table S2; see *SI Materials and Methods* for details) with

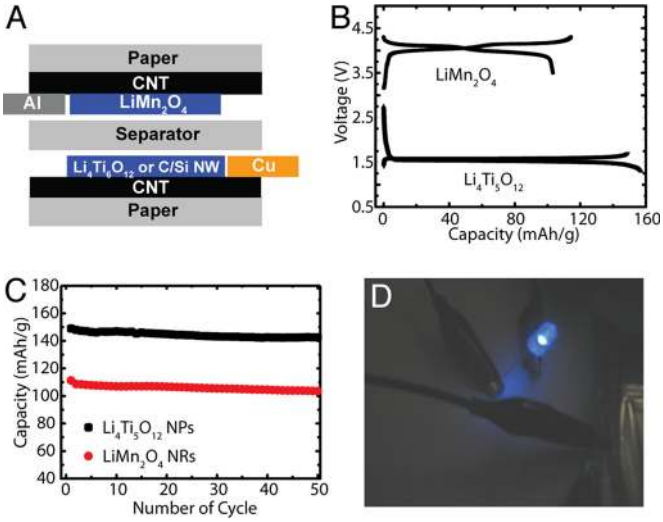

Fig. 4. Conductive paper as the current collector for Li-ion batteries. (*A*) Schematic illustration of the conductive paper battery configuration. The metal leads contact only CNTs but not active materials. Lithium foil is used as the counter electrode in half-cell tests. (*B*) Galvanostatic charging/discharging curves of $LiMn_2O_4$ nanorod cathode (3.5–4.3 V) and $Li_4Ti_5O_{12}$ nanopowder anode (1.3–1.7 V) half-cells with conductive paper current collectors. The current rate is C/5. (*C*) Cycling performance of $LiMn_2O_4$ nanorod (C/3, 49 mA/g) and $Li_4Ti_5O_{12}$ nanopowder (C/3, 58 mA/g) half-cells. (*D*) A 5 cm^2 paper battery (a full cell with $LiMn_2O_4$ nanorod cathode, C/Si core/shell NW anode, and conductive paper current collectors) used to repeatedly light up a blue LED.

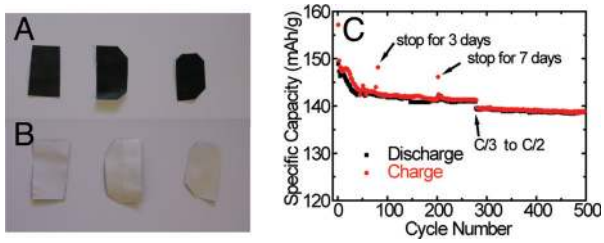

Fig. 5. Tests on the stability of paper in the organic electrolyte. The side with CNTs (*A*) and without CNTs (*B*) of the conductive paper soaked in organic electrolyte (1 M $LiPF_6$ in EC/DEC). From left to right: as-coated conductive paper, paper soaked for 2 months at 30 °C, and paper soaked for 1 month at 50 °C. (*C*) A total of 500 cycles of $Li_4Ti_5O_{12}$ nanopowders with conductive paper as the current collector. The mass loading of $Li_4Ti_5O_{12}$ is ≈2 mg/cm^2. The total time is about 3.5 months.

reasonable internal resistance (Fig. S7), even considering the weight of all components in a battery. Hence, higher gravimetric energy density can be achieved in such paper batteries. Previously, Pushparaj et al. (25) fabricated "paper batteries" with CNTs themselves as the active electrode material for Li-ion batteries. However, as an active material, CNTs suffer from issues of poor initial Coulomb efficiency, unsuitable voltage profiles, and fast-capacity decay (25, 37). Instead of using the CNTs to store lithium ions, we used them to function as lightweight current collectors to achieve practical batteries with a long cycle life. Fig. 4*A* shows the structure of conductive paper-based battery. $LiMn_2O_4$ nanorods (38) and $Li_4Ti_5O_{12}$ nanopowders (≈200 nm; Süd Chemie) or Si/C (39) nanowires were coated onto conductive paper to act as the cathode and anode, respectively. Fig. 4*B* displays the initial charge/discharge curves of half cells consisting of the $LiMn_2O_4$ nanorods or $Li_4Ti_5O_{12}$ nanopowders coated on conductive paper as working electrodes and lithium foil as counter electrodes. Voltage profiles were close to those with metal current collectors, according to previous work, and no apparent voltage drop was observed (38, 40–42). The cycling performance of these conductive paper-supported electrodes is shown in Fig. 4*C*. The $LiMn_2O_4$ nanorod and $Li_4Ti_5O_{12}$ nanopowder electrodes achieved initial discharge capacities of 110 mAh/g and 149 mAh/g, and capacity retentions of 93% and 96% after 50 cycles at C/3, respectively. These values are comparable with metal collector-based batteries (38, 40–42). In our devices, the coulomb efficiency was generally ≈98.5% for $LiMn_2O_4$ and over 99.5% for $Li_4Ti_5O_{12}$. To demonstrate a practical paper battery, a 5 cm^2 full cell with conductive paper acting as the current collector in both cathode and anode was used to repeatedly light a blue LED, as shown in Fig. 4*D*. In this demonstration, the cathode is $LiMn_2O_4$, whereas the anode is carbon/silicon core/shell nanowires.

The chemical stability of conductive paper in the electrolyte may be a main concern for practical uses. Paper has been used as the separator in aluminum electrolytic capacitors with aqueous solution (43), and our tests also show that paper is stable in aqueous electrolyte (1 M H_2SO_4) for 2 months. Regarding organic electrolyte, the stability of paper is tested under both component and device levels. After soaking the CNT conductive paper in organic electrolyte [1 M $LiPF_6$ in ethylene carbonate/diethyl carbonate (EC/DEC)] at 30 °C for 2 months or 50°C for 1.5 months, there was no detectable disintegration of paper and CNTs (Fig. 5 *A* and *B*). Moreover, the sheet resistance of the conductive paper decreased from ≈60 Ω/sq down to 9 Ω/sq after soaking in the organic electrolyte, which might be due to the dissolution of surfactant or hole doping of CNTs (44). On the device level, batteries with CNT conductive paper as current collectors were cycled 500 times, as shown in Fig. 5*C*. The capacity retention was 95% after 280 cycles at C/3. Moreover, during the following 220 cycles at the rate of C/2, the capacity decay was less than 0.01% per cycle. The total time for the 500 cycles is ≈3.5 months. In addition, after stopping cycling for a week, the charge capacity only increased by 3.3%, indicating that there is not much self-discharge for batteries with paper-based batteries. These experiments demonstrate that paper is stable in electrolyte for at least months, and the stable period of paper in organic electrolyte could further extend to more than 1 year, which is close to the shelf life requirement for some applications.

Conclusion

In conclusion, we have made highly conductive CNT paper by conformal coating of CNTs onto commercial paper, whose conductivity can be further enhanced by incorporating metal nanowire strips as global current collectors for large-scale energy-storage devices (Figs. S4*D*). The intrinsic properties of paper, such as high solvent absorption and strong binding with nanomaterials, allow easy and scalable coating procedures. Taking advantage of the mature paper technology, low cost, light and high-performance energy-storage devices are realized by using conductive paper as current collectors and electrodes. The concept of using paper as a novel substrate together with solution-processed nanoscale materials could bring in new opportunities for advanced applications in energy storage and conversion. By combining our paper-based energy storage with other types of devices developed, such as bioassays or displays on paper, full paper electronics could be realized in the future.

Materials and Methods

Preparation of Inks and Conductive Paper. To form a CNT ink, CNTs grown by laser ablation and SDBS (Sigma–Aldrich) were dispersed in deionized water. Their concentrations were 10 and 1–5 mg/mL, respectively. After bath sonication for 5 min, the CNT dispersion was probe-sonicated for 30 min at 200 W (VC 505; Sonics) to form an ink. Meyer rods (Rdspecialties) were used to coat the CNT ink onto Xerox paper. The sheet resistance of conductive paper was measured by using the four-point probe technique (EDTM). To make silver nanowire (Ag NW) ink, Ag NWs were produced in solution phase following the method of Xia and colleagues (45). In the first step, a mixture of 0.668 g of polyvinylpyrrolidone (PVP) and 20 mL of ethylene glycol (EG) was heated in a flask at 170 °C. Once the temperature was stabilized, 0.050 g of silver chloride

(AgCl) was ground finely and added to the flask for initial nucleation. After 3 minutes, 0.22 g of silver nitrate ($AgNO_3$) was titrated for 10 minutes. Then, the flask was kept at the same temperature for another 30 minutes. After the reaction was completed, the solution was cooled down and centrifuged three times to remove solvent, PVP, and other impurities.

Cell Preparation and Measurements of SCs. For aqueous electrolyte devices, two pieces of CNT conductive paper were first attached on glass slides. CNT films were used as both electrodes and current collectors. At the end of the CNT paper, a small piece of platinum was clipped onto the CNT conductive paper by a toothless alligator clip to connect to a battery analyzer (Maccor 4300). Both glass slides were assembled with a separator (Whatman 8-μm filter paper) sandwiched in between. The paper assembly was wrapped with parafilm and then dipped in the electrolyte solution. The active area overlapped by both CNT conductive papers was 1 cm^2. For organic electrolyte devices, cells were assembled by inserting the same separator soaked with the standard battery electrolyte (1 M $LiPF_6$ in ethylene carbonate:diethylene carbonate = 1:1 vol/vol; Ferro) between two CNT conductive paper substrates. The active area overlapped by both CNT conductive paper substrates was also 1 cm^2. Then, the entire assembly was sealed in a polybag (Sigma–Aldrich). As in the aqueous cells, small pieces of platinum were attached to the end of CNT conductive paper for a good electrical contact. The current collectors came out through the sealed edges of polybags and then were connected to the battery analyzer. All steps in the cell preparation were done in an argon-filled glove box (oxygen and water contents below 1 and 0.1 ppm, respectively). Typical mass loadings for data shown in the main text Fig. 3 *C* and *D* are 72 $\approx$ 270 $\mu g/cm^2$. Larger mass loadings up to 1.7 mg/cm^2 were also tested (Fig. 3 *D* and *E*, and Fig. S6*C*), and the capacitances are plotted in Fig. S6. Capacitance, energy density, and power density are all characterized by galvanostatic measurements. A total of 0.02 $\approx$ 20 mA/cm^2 were applied to cells while potentials between both electrodes swept between cutoff values ($0 \leq V \leq 0.85 \approx 1$ V in aqueous phase, $0 \leq V \leq 2.3 \approx 3$ V in organic phase). Voltages were recorded every 0.01 $\approx$ 0.2 seconds. For the cycling test in both phases of electrolyte, $\approx$5 A/g was applied. The cutoff potentials for the sulfuric acid and organic electrolyte were 0.85 and 2.3 V, respectively.

Battery Fabrication and Test. The cathode materials $LiMn_2O_4$ nanorods were synthesized according to our previous work, with modification (38). Typically, 8 mmol $MnSO_4{\cdot}H_2O$ and 8 mmol $(NH_4)_2S_2O_8$ were dissolved in 20 mL of deionized water, and the solution was transferred to a 45-mL, Teflon-lined stainless steel vessel (Parr). The vessel was sealed and heated at 150 °C for 12 h to obtain β-MnO_2 nanorods. The as-synthesized MnO_2 nanorods were mixed and ground with lithium acetate (Aldrich) at a molar ratio of 2:1. A total of 1 mL of methanol was added to make a uniform slurry mixture. Then, the mixture was sintered at 700 °C for 10 h under air to obtain $LiMn_2O_4$ nanorods. The carbon/silicon core/shell nanowires were synthesized by CVD method. Carbon nanofibers (Sigma–Aldrich) were loaded into a tube furnace and heated to 500 °C. Then, silane gas was introduced and decomposed onto carbon nanofibers. The weight ratio of silicon shell to carbon core was typically $\approx$2:1. $Li_4Ti_5O_{12}$ powder was used as received from Süd Chemie.

Electrodes for electrochemical studies of $LiMn_2O_4$ and $Li_4Ti_5O_{12}$ were prepared by making slurry of 70 wt % active materials, 20 wt % Super P Carbon, and 10 wt % PVDF binder in *N*-methyl-2-pyrrolidone (NMP) as the solvent. The slurry was coated onto a piece of conductive CNT paper by an applicator and then dried at 100 °C in a vacuum oven overnight. For C/Si core/shell nanowires, the as-synthesized nanowires were dropped onto a CNT paper and dried to form the anode.

The half-cell tests of both cathode ($LiMn_2O_4$) and anode ($Li_4Ti_5O_{12}$) were carried out inside a coffee bag (pouch) cell assembled in an argon-filled glovebox (oxygen and water contents below 1 and 0.1 ppm, respectively). Lithium metal foil (Alfa Aesar) was used as the counter electrode in each case. A 1 M solution of $LiPF_6$ in EC/DEC (1:1 vol/vol; Ferro) was used as the electrolyte, with separators from Asahi Kasei. The charge/discharge cycles were performed at different rates at room temperature, where 1C was 148 mA/g for $LiMn_2O_4$ and 175 mA/g for $Li_4Ti_5O_{12}$, respectively. The voltage range was 3.5–4.3 V for $LiMn_2O_4$ and 1.3–1.7 V for $Li_4Ti_5O_{12}$. Tests were performed by either Bio-Logic VMP3 battery testers or MTI battery analyzers. To fabricate a full cell with high voltage to light a blue LED, silicon/carbon core/shell nanowires and $LiMn_2O_4$ nanorods were used as anode and cathode, respectively. Then, the two electrodes were assembled to make a 5 cm^2 pouch cell as described above, and it was used to repeatedly light the blue LED.

ACKNOWLEDGMENTS. This work was supported by The Korea Foundation for Advanced Studies (S.J.) and King Abdullah University of Science and Technology Investigator Award KUS-I1-001-12 (to Y.C.).

1. Ahn JH, et al. (2006) Heterogeneous three-dimensional electronics by use of printed semiconductor nanomaterials. *Science* 314:1754–1757.
2. Talapin DV, Murray CB (2005) PbSe nanocrystal solids for n- and p-channel thin film field-effect transistors. *Science* 310:86–89.
3. Duan XF, et al. (2003) High-performance thin-film transistors using semiconductor nanowires and nanoribbons. *Nature* 425:274–278.
4. Kim JY, et al. (2007) Efficient tandem polymer solar cells fabricated by all-solution processing. *Science* 317:222–225.
5. Bach U, et al. (1998) Solid-state dye-sensitized mesoporous TiO2 solar cells with high photon-to-electron conversion efficiencies. *Nature* 395:583–585.
6. An KH, et al. (2001) Supercapacitors using single-walled carbon nanotube electrodes. *Adv Mater* 13:497–500.
7. Poizot P, et al. (2000) Nano-sized transition-metaloxides as negative-electrode materials for lithium-ion batteries. *Nature* 407:496–499.
8. Edwards IES, Hammond NGL, Gadd CJ (1975) *The Cambridge Ancient History* (Cambridge Univ Press, Cambridge, UK).
9. Roberts JC (1996) *Paper Chemistry* (Springer, New York).
10. Martinez AW, Phillips ST, Whitesides GM (2008) Three-dimensional microfluidic devices fabricated in layered paper and tape. *Proc Natl Acad Sci USA* 105:19606–19611.
11. Carrilho E, Martinez AW, Whitesides GM (2009) Understanding wax printing: A simple micropatterning process for paper-based microfluidics. *Anal Chem* 81:7091–7095.
12. Lamprecht B, et al. (2005) Organic photodiodes on newspaper. *Physica Status Solidi A* 202:R50–R52.
13. Kaihovirta NWC, Makela T, Wilen C, Osterbacka R (2009) Self-supported ion-conductive membrane-based transistors. *Adv Mater* 21:2520–2523.
14. Eder F, et al. (2004) Organic electronics on paper. *Appl Phys Lett* 84:2673–2675.
15. Kim DHK, et al. (2009) Ultrathin silicon circuits with strain-isolation layers and mesh layouts for high-performance electronics on fabric, vinyl, leather, and paper. *Adv Mater* 21:3703–3707.
16. Anderson P, et al. (2002) Active matrix displays based on all-organic electrochemical smart printed on paper. *Adv Mater* 14:1460–1464.
17. Islam MF, et al. (2003) High weight fraction surfactant solubilization of single-wall carbon nanotubes in water. *Nano Lett* 3:269–273.
18. Kordas K, et al. (2006) Inkjet printing of electrically conductive patterns of carbon nanotubes. *Small* 2:1021–1025.
19. Hecht DS, Hu L, Gruner G (2007) Electronic properties of carbon nanotube/fabric composites. *Curr Appl Phys* 7:60–63.
20. Doherty EDS, et al. (2009) The spatial uniformity and electromechanical stability of transparent, conductive films of single walled nanotubes. *Carbon* 47:2466–2473.
21. Hu L, Hecht DS, Gruner G (2004) Percolation in transparent and conducting carbon nanotube networks. *Nano Lett* 4:2513–2517.
22. Gutoff EB, Cohen ED (2006) *Coating and Drying Defects*: *Troubleshooting Operating Problems* (*Society of Plastics Engineers Monographs*), (John Wiley & Sons, Hoboken, NJ).
23. Hertel T, Walkup REAP (1998) Deformation of carbon nanotubes by surface van der Waals forces. *Phys Rev B* 58:13870–13873.
24. Endo M, et al. (2005) 'Buckypaper' from coaxial nanotubes. *Nature* 433:476–476.
25. Pushparaj VL, et al. (2007) Flexible energy storage devices based on nanocomposite paper. *Proc Natl Acad Sci USA* 104:13574–13577.
26. Kaempgen M, et al. (2009) Printable thin film supercapacitors using single-walled carbon nanotubes. *Nano Lett* 9:1872–1876.
27. Kimizuka O, et al. (2008) Electrochemical doping of pure single-walled carbon nanotubes used as supercapacitor electrodes. *Carbon* 46:1999–2001.
28. Futaba DN, et al. (2006) Shape-engineerable and highly densely packed single-walled carbon nanotubes and their application as super-capacitor electrodes. *Nat Mater* 5:987–994.
29. Du CS, Pan N (2006) Supercapacitors using carbon nanotubes films by electrophoretic deposition. *J Power Sources* 160:1487–1494.
30. Ma RZ, et al. (1999) Processing and performance of electric double-layer capacitors with block-type carbon nanotube electrodes. *Bull Chem Soc Jpn* 72:2563–2566.
31. Zhou CF, Kumar S, Doyle CD, Tour JM (2005) Functionalized single wall carbon nanotubes treated with pyrrole for electrochemical supercapacitor membranes. *Chem Mater* 17:1997–2002.
32. Ahn HJ, et al. (2006) Electrochemical capacitors fabricated with carbon nanotubes grown within the pores of anodized aluminum oxide templates. *Electrochem Comm* 8:513–516.
33. Niu CM, et al. (1997) High power electrochemical capacitors based on carbon nanotube electrodes. *Appl Phys Lett* 70:1480–1482.
34. Malinauskas A, Malinauskiene J, Ramanavicius A (2005) Conducting polymer-based nanostructurized materials: Electrochemical aspects. *Nanotechnology* 16:R51–R62.
35. An KH, et al. (2002) High-capacitance supercapacitor using a nanocomposite electrode of single-walled carbon nanotube and polypyrrole. *J Electrochem Soc* 149:A1058–A1062.
36. Pandolfo AG, Hollenkamp AF (2006) Carbon properties and their role in supercapacitors. *J Power Sources* 157:11–27.
37. Landi BJ, et al. (2008) Lithium ion capacity of single wall carbon nanotube paper electrodes. *J Phys Chem C* 112:7509–7515.
38. Yang Y, et al. (2009) Single nanorod devices for battery diagnostics: A case study of $LiMn_2O_4$. *Nano Lett*, in press.
39. Cui LF, Yang Y, Hsu CM, Cui Y (2009) Carbon-silicon core-shell nanowires as high capacity electrode for lithium ion batteries. *Nano Lett* 9:3370–3376.
40. Kavan L, Gratzel M (2002) Facile synthesis of nanocrystalline Li4Ti5O12 (spinel) exhibiting fast Li insertion. *Electrochem Solid State Lett* 5:A39–A42.
41. Zaghib K, Simoneau M, Armand M, Gauthier M (1999) Electrochemical study of Li4Ti5O12 as negative electrode for Li-ion polymer rechargeable batteries. *J Power Sources* 81:300–305.
42. Thackeray MM, et al. (1984) Electrochemical extraction of lithium from Limn2o4. *Mater Res Bull* 19:179–187.
43. Muriset G (1952) Influence of the impurities in the foil, electrolyte and paper in the electrolytic capacitor. *J Power Source* 99:285–288.
44. Zhou WVJ, et al. (2005) Charge transfer and Fermi level shift in p-doped single-walled carbon nanotubes. *Phys Rev B* 71:205423.
45. Sun YG, Mayers B, Herricks T, Xia YN (2003) Polyol synthesis of uniform silver nanowires: A plausible growth mechanism and the supporting evidence. *Nano Lett* 3:955–960.